Charge symmetry violation in the determination of strangeness form factors

Ali Alkathiri ⊙

CSSM, School of Physical Sciences, University of Adelaide, Adelaide SA 5005, Australia
and Physics Department, Taif University, Taif 26571, Saudi Arabia

Ross D. Young ⊙ and James M. Zanotti ⊙

CSSM, School of Physical Sciences, University of Adelaide, Adelaide SA 5005, Australia

The strange quark contributions to the electromagnetic form factors of the proton are ideal quantities to study the role of hidden flavor in the properties of the proton. This has motivated intense experimental measurements of these form factors. A major remaining source of systematic uncertainty in these determinations is the assumption that charge symmetry violation (CSV) is negligible. We use recent theoretical determinations of the CSV form factors and reanalyze the available parity-violating electron scattering data, up to $Q^2 \approx 1$ GeV^2. Our analysis considers systematic expansions of the strangeness electric and magnetic form factors of the proton. The results provide an update to the determination of strangeness over a range of Q^2 where, under certain assumptions about the effective axial form factor, an emergence of nonzero strangeness is revealed in the vicinity of $Q^2 \approx 0.6$ GeV^2. Given the recent theoretical calculations, it is found that the current limits on CSV do not have a significant impact on the interpretation of the measurements and hence suggests an opportunity for a next generation of parity-violating measurements to more precisely map the distribution of strange quarks.

I. INTRODUCTION

The desire for a complete understanding of the electromagnetic structure of the proton has led to significant efforts over the last two decades to determine the individual quark flavor contributions to the proton's electromagnetic form factors. A significant challenge in this goal lies in determining the role played by nonvalence or hidden quark flavors whose contributions arise only through fluctuations of the QCD vacuum. Being the lightest sea-only quark, strange quarks are anticipated to make the most significant contribution. Through an extensive experimental program of parity-violating electron scattering (PVES) [1–12], strange quarks have been tagged by measuring the neutral-current form factors. The isolation of strangeness relies on the assumption of good charge symmetry, which has been one of the limiting factors in extending the experimental program to greater precision. In this work, we quantify the impact of charge symmetry violation (CSV) on the extraction of strangeness from a global analysis of the PVES measurements.

While earlier theoretical predictions of CSV in the proton's electromagnetic form factors varied through orders of magnitude [13–18], a recent lattice QCD calculation [19] has determined that CSV in the proton's electromagnetic form factors is significantly smaller than earlier expectations. While this recent calculation seems to support analyses, which invoke exact charge symmetry, other models suggest considerable violation of this symmetry. The effects of this violation have yet to be quantified. Hence, here we perform a global analysis of the full existing set of parity-violating (PV) asymmetry data with and without the constraint of CSV form factors. To achieve this task, we consider PVES data, obtained from experiments conducted with varying kinematics and targets, from SAMPLE [1,2], PVA4 [3–5], HAPPEX [6–10], G0 [11,12], and Q$_{\text{weak}}$ [20].

This paper is organized as follows: In Sec. II, we describe the formalism of PVES, including PV asymmetries of the nucleon, helium-4, and the deuteron. Section III presents the parametrization of strange quark form factor, while Sec. IV is dedicated to a study of the CSV effects on strangeness form factor extraction. A brief summary is finally presented in Sec. V.

II. STRANGE FORM FACTORS AND PARITY-VIOLATING ELECTRON SCATTERING

Determining the strange electric and magnetic form factors experimentally requires a process where the weak and electromagnetic interactions interfere. This is achieved through PVES experiments [21,22], whose leading-order amplitudes are shown in Fig. 1.

Under the assumption of charge symmetry, the PV asymmetry in polarized *e-p* scattering is given by [23]

$$A_{\text{PV}}^p = \left[\frac{-G_F Q^2}{4\sqrt{2}\pi\alpha} \right] \left(A_V^p + A_s^p + A_A^p \right), \quad (1)$$
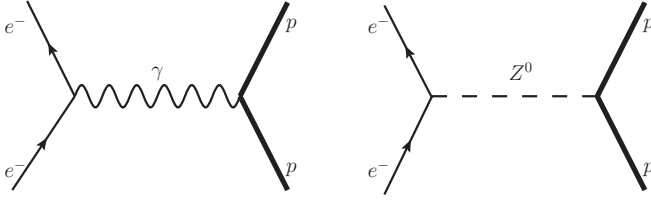
FIG. 1. Total leading-order amplitude for electron-nucleon scattering is the sum of the leading-order electromagnetic and neutral current amplitudes.

where in terms of the proton's electric ($G_E^{\gamma,p}$) and magnetic ($G_M^{\gamma,p}$) Sach's form factors

$$A_V^p = (1 - 4 \sin^2 \hat{\theta}_w)(1 + R_V^p)$$
$$- (1 + R_V^n)\frac{\epsilon G_E^{\gamma,p} G_E^{\gamma,n} + \tau G_M^{\gamma,p} G_M^{\gamma,n}}{\epsilon (G_E^{\gamma,p})^2 + \tau (G_M^{\gamma,p})^2}, \quad (2)$$

$$A_s^p = -(1 + R_V^{(0)})\frac{\epsilon G_E^{\gamma,p} G_E^s + \tau G_M^{\gamma,p} G_M^s}{\epsilon (G_E^{\gamma,p})^2 + \tau (G_M^{\gamma,p})^2}, \quad (3)$$

and

$$A_A^p = \frac{-\epsilon'(1 - 4 \sin^2 \hat{\theta}_W)G_M^{\gamma,p} \tilde{G}_A^{e,p}}{\epsilon (G_E^{\gamma,p})^2 + \tau (G_M^{\gamma,p})^2}, \quad (4)$$

are the proton's vector form factor excluding strangeness (A_V^p), the proton's strangeness vector form factor (A_s^p), and the interference of the proton's magnetic vector, and the axial vector form factors (A_A^p).

The electromagnetic form factors of the proton and neutron are denoted by $G_{E,M}^\gamma$, the strangeness vector form factors $G_{E,M}^s$, and the effective axial form factor $\tilde{G}_A^p$. The kinematic variables, which depend on the four-momentum transfer $Q^2 = -q^2$ and the electron scattering angle θ, are defined as

$$\tau = \frac{Q^2}{4M_p^2}, \quad (5)$$

$$\epsilon = \frac{1}{1 + 2(1 + \tau)\tan^2 \frac{\theta}{2}}, \quad (6)$$

and

$$\epsilon' = \sqrt{\tau(1 + \tau)(1 - \epsilon^2)}, \quad (7)$$

where M_p, ϵ and ϵ' are the proton's mass, the virtual photon longitudinal polarization and the scattered energy, respectively. The standard model parameters: fine structure constant α, Fermi coupling $G_F = 1.16638 \times 10^{-5}\,\mathrm{GeV}^2$, and the weak mixing angle, $\sin^2 \hat{\theta}_W = 0.23129(5)$, in the $\overline{\mathrm{MS}}$ renormalization scheme are all obtained from the PDG [24]. The standard model radiative corrections, following notation of Ref. [23], take the values $R_V^p = -0.0513(40)$ and $R_V^n = R_V^{(0)} = -0.0098(3)$ are adopted from Ref. [25].

A. Helium-4 and deuteron PV asymmetries

The ^{4}He nucleus is spin zero, parity even, and isoscalar. Elastic electron scattering from ^{4}He is an isoscalar $0^+ \to 0^+$

transition and therefore allows no contributions from magnetic or axial-vector currents. Thus, the HAPPEX Collaboration has utilized a ^{4}He target to directly extract the strange electric form factor [6]. Nuclear corrections are relevant for ^{4}He and deuteron targets, more details about which can be found in Refs. [26,27].

Following this original experimental analyses, we first consider the ^{4}He asymmetry in the absence of isospin mixing is written as [23]

$$A_{\mathrm{PV}}^{\mathrm{He}} = -\left[\frac{G_F Q^2}{4\sqrt{2}\pi\alpha}\right] \cdot \left[(1 - 4\sin^2\theta_w)(1 + R_V^p)\right.$$
$$\left. - (1 + R_V^n) + 2\frac{-(1 + R_V^{(0)})G_E^s}{G_E^p + G_E^n}\right]. \quad (8)$$

The nuclear isospin violating corrections, explored in detail in Ref. [28], will be incorporated in Sec. IV.

The parity-violating asymmetries measured in quasielastic scattering from the deuteron have responses, which involve the deuteron wave functions. For this analysis, we use directly the theoretical asymmetries as reported with original experimental measurements. Early results from SAMPLE have had minor modifications made to update for more recent radiative corrections and form factor parameterizations, as described in Ref. [29].

B. γZ-exchange corrections to PVES

Leading electroweak corrections play a significant role in precision measurements of the strangeness contribution to the nucleon form factors [23,30]. In contrast to the formalism relevant to atomic parity violation experiments [31], an energy-dependent correction arising from the γZ box diagram was highlighted by Gorchtein and Horowitz [32]. The size of this correction is particularly significant to the standard model test by the Q-weak experiment [33]. Fortunately, the uncertainties arising from the underlying γZ interference structure functions can be reliably constrained [34]. The model used to construct the relevant γZ structure functions is supported by direct measurement [34], neglecting nuclear correction arising from the deuteron target.

Owing to the smallness of the proton weak charge, the relative significance of the γZ box is enhanced, and has received considerable theoretical attention [34]. While significant for precision weak charge measurements, the γZ box is somewhat less pronounced in the determination of strangeness. Nevertheless, for example, the correction makes about $\approx \frac{1}{2}$-σ shift to the central value of the precise HAPPEX proton point at $Q^2 \approx 0.1\,\mathrm{GeV}^2$. We incorporate the corrections reported by the constrained model of Ref. [34], updated with the improved constraints of quark-hadron duality [35], and a momentum dependence as proposed in Ref. [36]. For completeness, a table of values is included in Appendix B.

The energy-dependent γZ box contributions have not been investigated in detail for the nuclear targets. Given the larger weak charges, and lower-precision measurements, these corrections are not anticipated to appreciably affect the extraction of strangeness; however, this remains to be quantified.

C. Theoretical asymmetries

In this work, a set of all available PV asymmetry data up to $Q^2 \approx 1 \text{ GeV}^2$, as summarized in Table IV, is analyzed. Such a combined analysis of the world PV data requires a consistent treatment of the vector and axial form factors and radiative corrections. The theoretical asymmetry used in this analysis is written as

$$A_{\text{Theory}} = \eta_0 + \eta_A^p \tilde{G}_A^p + \eta_A^n \tilde{G}_A^n + \eta_E G_E^s + \eta_M G_M^s, \quad (9)$$

where the η's, which can be read off from Eqs. (2)–(4), are provided in Table IV. These are calculated using the recent elastic form factor parametrizations of Ye *et al.* [37] and current values for the standard model radiative corrections [24]. The uncertainties associated with these parametrizations are no more than 2% and hence have negligible effects on the current analysis and thus have been disregarded.

In this analysis, since the entire contribution is to be fit to data, we employ the effective axial form factors $\tilde{G}_A^{p,n}$ which implicitly includes both the axial radiative and anapole corrections. For these form factors, we employ a dipole form

$$\tilde{G}_A^{p,n} = \tilde{g}_A^{p,n}\left(1 + \frac{Q^2}{M_A^2}\right)^{-2}, \quad (10)$$

with an axial dipole mass $M_A = 1.026 \text{ GeV}$, determined from neutrino scattering [38], common to both proton and neutron form factors. The normalizations $\tilde{g}^{p,n}$ are fit to the data, however, since the isoscalar combination is very poorly determined, we choose to impose theoretical estimates based on an effective field theory (EFT) with vector-meson dominance (VMD) model to constrain this combination [39]

$$\tfrac{1}{2}\left(\tilde{g}_A^p + \tilde{g}_A^n\right) = -0.08 \pm 0.26. \quad (11)$$

III. ANALYSIS FRAMEWORK

A. Taylor expansion

At low momentum transfers, a Taylor series expansion of the electromagnetic form factors in Q^2 is sufficient and minimizes the model dependence. Given the sparsity and precision of the available data—up to $\approx 1 \text{ GeV}^2$—we avoid introducing a specific model by first attempting to parameterise the strange electric and magnetic form factors Q^2 dependence by

$$G_E^s = \rho_s Q^2 + \rho_s' Q^4,$$
$$G_M^s = \mu_s + \mu_s' Q^2. \quad (12)$$

B. z expansion

A priori, one might not expect a Taylor expansion up to $\approx 1 \text{ GeV}^2$ to be satisfactory. To provide an alternative functional form to the Taylor expansion, we also consider the z expansion, which offers improved convergence based on the analytic properties of the form factors [40–42]. We describe the momentum dependence of the strange form factors using the z expansion, also to second (nontrivial) order:

$$G_E^s = \rho_{s,z} z + \rho_{s,z}' z^2,$$
$$G_M^s = \mu_s + \mu_{s,z}' z, \quad (13)$$

where

$$z = \frac{\sqrt{t_{\text{cut}} + Q^2} - \sqrt{t_{\text{cut}}}}{\sqrt{t_{\text{cut}} + Q^2} + \sqrt{t_{\text{cut}}}}. \quad (14)$$

In our fits, we use $t_{\text{cut}} = (2m_K)^2$, with the kaon mass $m_K = 0.494 \text{ GeV}$. In the absence of isospin violation, the cut formally starts at $9m_\pi^2$, but we assume that the strangeness contribution to the three-pion state can be neglected. We note that, with the current experimental precision, there is not any significant sensitivity to the value of t_{cut}. To more easily facilitate the comparison with the two expansion forms, we report the simple Taylor expansion coefficients for each case. That is, for the z fits, we translate the expansions back in the leading Taylor form, e.g., $\rho_s = dG_E^s/dQ^2|_{Q^2=0}$.

C. Dipole form

For completeness, we examine our fits against the dipole(like) form

$$G_E^s = \rho_s Q^2\left(1 + \frac{Q^2}{\Lambda^2}\right)^{-2},$$
$$G_M^s = \mu_s\left(1 + \frac{Q^2}{\Lambda^2}\right)^{-2}, \quad (15)$$

where taken as $\Lambda = 1 \text{ GeV}$.

D. Charge symmetry results

Here we summarize the fit results under the assumption of exact charge symmetry. This provides a baseline with which to explore the implications of charge symmetry violation in the following section.

In this work we perform a global fit at leading order (LO) and at next-leading order (NLO) of the strangeness form factor. Thus, the fitting procedure at LO considers four parameters, $\tilde{g}_A^p$, $\tilde{g}_A^n$, μ_s, and ρ_s, while fitting at NLO considers an additional two parameters, μ_s' and ρ_s'. The theoretical constraint on the isoscalar form factor, Eq. (11), is incorporated by adding an additional data point to the analysis.

The χ^2 is calculated as

$$\chi^2 = \sum_i \sum_j (m_i - t_i)(V)_{ij}^{-1}(m_j - t_j), \quad (16)$$

where m and t denote the measurement and theory asymmetry, respectively. The indices i and j run over the data ensemble. The matrix V represents the covariance error matrix defined as

$$(V)_{ij} = \left(\sigma_i^{\text{uncor}}\right)^2 \delta_{ij} + \sigma_i^{\text{cor}}\sigma_j^{\text{cor}}, \quad (17)$$

where σ_i^{uncor} and σ_i^{cor} are uncorrelated and correlated uncertainties of the ith measurement, respectively. We note that the correlated uncertainties are only relevant for the G0 experiment, where the forward [11] and backward [12] data are treated as mutually independent, see Table IV. The goodness of fit is estimated from the reduced χ^2 as

$$\chi_{\text{red}}^2 = \chi^2/\text{d.o.f.}, \quad (18)$$

TABLE I. The parameter values and χ^2 obtained from previous PVES global fits [29,43–45] and the current global analysis at LO for both Taylor and z-expansion form factor fits without constraints from CSV.

	ρ_s (GeV^{-2})	μ_s	χ^2_{red}
YRCT(2006) [29]	-0.06 ± 0.41	0.12 ± 0.55	1.3
YRCT(2007) [44]	0.02 ± 0.18	-0.01 ± 0.25	–
LMR(2007) [45]	-0.08 ± 0.16	0.29 ± 0.21	1.3
GCD(2014) [43]	0.26 ± 0.16	-0.26 ± 0.26	1.3
Taylor	0.15 ± 0.04	-0.12 ± 0.04	1.1
z exp.	0.18 ± 0.05	-0.10 ± 0.04	1.1

with 33 and 31 degrees of freedom (d.o.f.) for the LO and NLO fits, respectively.

We report the leading-order fit results in Table I, with comparisons against previous work. The results are compatible with earlier work, though with significantly reduced uncertainty. This is due to both an updated list of measurements and the inclusion of the full range of Q^2 points in the fit. No appreciable difference is seen between the simple Taylor expansion and the z expansion.

While the fit quality is reasonable, these simple leading-order fits are certainly anticipated to be too simple to describe these form factors over the full range $0 \leqslant Q^2 \lesssim 1.0$ GeV^2. As a result, the statistical uncertainties displayed are not representative of the current knowledge of the strange form factors. We hence allow for more variation in the Q^2 dependence by extending the fits to next-leading order, Eqs. (12) and (13). Results are shown in Table II. Curiously the additional fit parameters are unable to make significant improvement to the χ^2 and the reduced χ^2 very marginally increases for the NLO fit.

Clearly the data are unable to constrain the additional fit parameters. Given the clustering of the underlying data set, the separation of the electric and magnetic strange form factors is most reliable at the discrete momentum transfers near $Q^2 \approx 0.1, 0.2$, and 0.6 GeV^2. A completely model-independent extraction would hence only determine the form factors at these points. To smoothly interpolate these three points, at best one can only constrain two free parameters (for each form factor). As a tradeoff from the physically unsatisfactory constant G_M^s and slope-only G_E^s, we prefer NLO results as a better representation of the underlying uncertainties.

The comparison between the leading- and next-to-leading-order fits for the Taylor expansion are shown in Fig. 2 together with the dipole form fits. As can been noted, these fits produce similar results around $Q^2 \approx 0.6$ GeV^2 for both G_E^s and G_M^s.
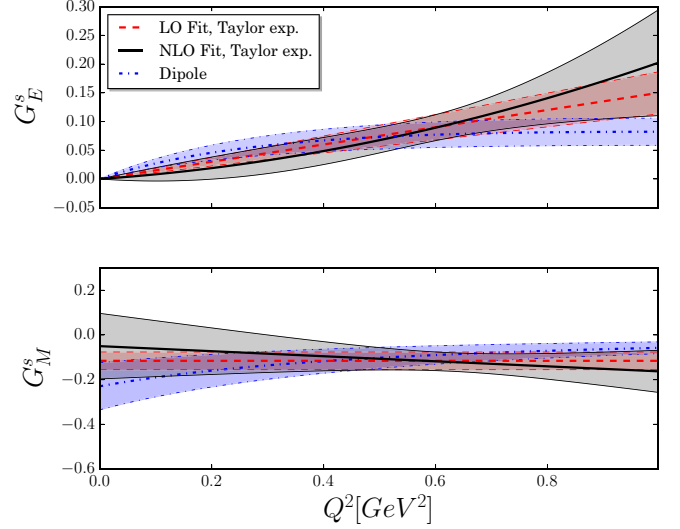

FIG. 2. The extracted strange electric and magnetic form factors from a global fit up to $Q^2 \approx 1$ GeV^2. The Taylor expansions, Eq. (12), at leading order is shown by the red (dashed) curves and next-to-leading order by the black (solid) curves. The dipole forms, Eq. (15), are shown by the blue (dot-dashed) curves. The shaded areas indicate the uncertainties of G_E^s and G_M^s.

The corresponding z-expansion results are very similar. In Fig. 3 we show the NLO z-expansion parametrization of the separated electric and magnetic form factors and compare with recent lattice QCD results [46,47]. Here we observe excellent agreement between our strangeness determination based on PVES data and lattice QCD results over the full Q^2 range. These are also compatible with earlier lattice [48] and lattice-constrained [49–51] results. Interestingly, we note that the experimental results are showing some support for a nonvanishing strangeness electric form factor in the vicinity of $Q^2 \approx 0.6$ GeV^2. Given the lack of sensitivity to the choice of functional form, we adopt the z expansion at NLO as our preferred fit for the following discussions. For completeness, a table of the correlation coefficients between the free parameters of the NLO z-expansion fit is presented in Appendix C.

The preceding discussion has focused on the separation of the electric and magnetic strangeness form factors. Given the high degree of correlation in the measurements, it is instructive to display the joint confidence intervals. Figure 4 displays the 95% confidence level ellipses for the different values of $Q^2 = 0.1, 0.23$, and 0.63 GeV^2 for the NLO z-expansion fit. At the low Q^2 values, we observe that the strangeness form factors are compatible with zero at the 95% CL, with a marginal preference for positive values of strange

TABLE II. The NLO parameters values and χ^2 obtained from a previous global fit [29], where $Q^2 < 0.3$ GeV^2, and the current global analysis at NLO for both Taylor and z-expansion form factor fits without constraints from CSV.

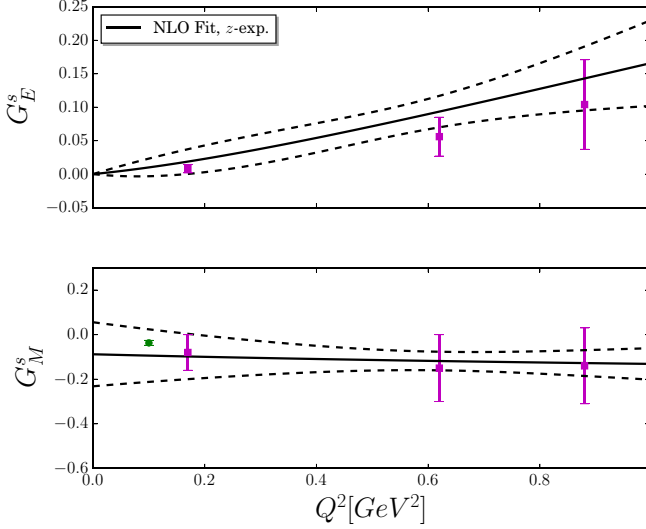|	ρ_s (GeV^{-2})	ρ_s' (GeV^{-4})	μ_s	μ_s' (GeV^{-2})	χ^2_{red}
YRCT(2006) [29]	-0.03 ± 0.63	-1.5 ± 5.8	0.37 ± 0.79	0.7 ± 6.8	1.4
Taylor	0.07 ± 0.14	0.14 ± 0.22	-0.05 ± 0.15	-0.11 ± 0.23	1.23
z exp.	0.08 ± 0.17	0.19 ± 0.37	-0.09 ± 0.14	-0.06 ± 0.29	1.26

FIG. 3. The extracted strange electric and magnetic form factors from global fit up to $Q^2 \approx 1$ GeV^2 with using the NLO z expansion in Eq. (13). A comparison with recent lattice QCD results is shown where the green square (errors bars smaller than the symbol) corresponds to the result of $G_M^s(Q^2 = 0.1$ GeV^2) [47] and the magenta squares are G_M^s and G_E^s at $Q^2 = 0.17$, 0.62, and 0.88 GeV^2 [46].

electric form factor and negative values of the magnetization, as seen earlier in Refs. [44,52].

At $Q^2 = 0.63$ GeV^2, there appears a clear signal for nonzero strangeness, with a negative G_M^s and positive G_E^s. In contrast to earlier work that has suggested vanishing strangeness at this Q^2 [10,12], the dominant difference in the present work is the treatment of the axial/anapole form factor. As described, the isoscalar combination is constrained by the EFT and VMD estimate of Zhu *et al.* [39], while the isovector combination is determined by the data. The best fit—for z expansion at NLO—results in $\tilde{g}_A^p = -0.67 \pm 0.25$, which is less negative than the zero-anapole approximation.
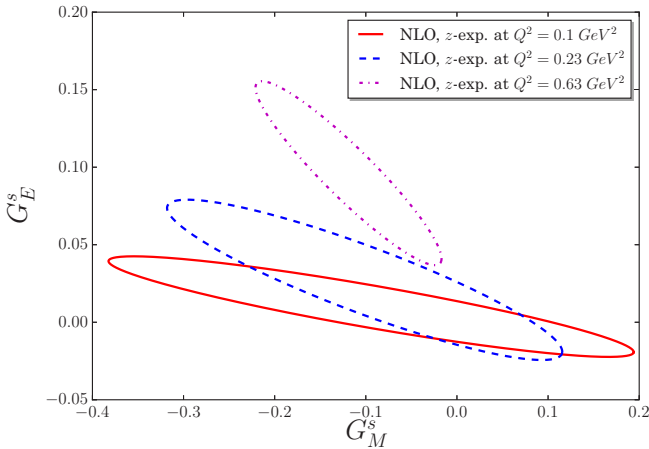

FIG. 4. 95% confidence level ellipses for the electric and magnetic strangeness form factors using the NLO z expansion in Eq. (13) for three Q^2 values 0.1 (red solid curve), 0.23 (blue dashed curve), 0.63 GeV^2 (magenta dot-dashed curve).

TABLE III. Strangeness form factor results at different values of $Q^2 = 0.1$, 0.23, and 0.63 GeV^2 against the variation of the axial dipole mass $M_A = 1.026 \pm 0.500$ GeV. The second quoted error bar indicates the sensitivity with the axial mass to the upper and lower mass scales. Correlation coefficients between the G_M^s and G_E^s are represented by ρ.

	$Q^2 = 0.1$ GeV^2	$Q^2 = 0.23$ GeV^2	$Q^2 = 0.63$ GeV^2
G_M^s	$-0.09(12)(4)$	$-0.10(8)(4)$	$-0.12(4)(6)$
G_E^s	$0.01(1)(0)$	$0.03(2)(0)$	$0.10(2)(2)$
ρ	-0.90	-0.90	-0.93

As a consequence, the data-driven fit drives the back-angle G0 results to be more consistent with a negative G_M^s. Under these assumptions for the effective axial form factor, we see $G_E^s \approx 0.1$, which, with the strange charge factor included ($G_E^{\gamma,p} = \frac{2}{3}G_E^{u,p} - \frac{1}{3}G_E^{d,p} - \frac{1}{3}G_E^{s,p}$), is on the order of 10% of the proton electric form factor at this momentum transfer. To investigate the effect of the uncertainty related to the axial form factor, a conservative variation of the axial mass M_A has been considered to be $M_A = 1.026 \pm 0.500$ GeV. It is found that some of the strangeness form factor results have differed as shown in Table III. The most significant shift is seen for G_M^s at the larger Q^2 point, yet still within 1-σ uncertainty and the conclusion derived from Fig. 4 still holds.

IV. SENSITIVITY TO CHARGE SYMMETRY VIOLATION

A. CSV in asymmetries

In this section we study the effects of charge symmetry violation on our results, i.e., we no longer have a relationship between the individual quark flavor contributions to the proton and neutron form factors

$$G_{E,M}^{p,u} \neq G_{E,M}^{n,d}, \quad G_{E,M}^{p,d} \neq G_{E,M}^{n,u}.$$

We follow standard notation and define the CSV form factors as

$$G_{E,M}^{\mathrm{CSV}} = \frac{2}{3}\left(G_{E,M}^{p,d} - G_{E,M}^{n,u}\right) - \frac{1}{3}\left(G_{E,M}^{p,u} - G_{E,M}^{n,d}\right). \quad (19)$$

In order to explore the impact of CSV, we need to modify the neutral weak form factors to explicitly include a CSV term

$$\begin{aligned} G_{E,M}^{Z,p} = &(1 - 4\sin^2\hat{\theta}_W)(1 + R_V^p)G_{E,M}^{\gamma,p} \\ &- (1 + R_V^n)G_{E,M}^{\gamma,n} - (1 + R_V^{(0)})G_{E,M}^s \\ &- (1 + R_V^n)G_{E,M}^{\mathrm{CSV}}, \end{aligned} \quad (20)$$

where the Q^2 dependence of each form factor has been dropped for clarity. The CSV form factor can be expressed as a simple Taylor expansion in Q^2

$$G_{E,M}^{\mathrm{CSV}}(Q^2) = G_{E,M}^{\mathrm{CSV}}(0) - \rho_{E,M}^{\mathrm{CSV}}Q^2 + \mathcal{O}(Q^4), \quad (21)$$

with G_E^{CSV} set to zero at $Q^2 = 0$ due to charge conservation.

Regarding the theoretical asymmetry given in Eq. (9), we note that η_0 will receive a correction due to the CSV form factor. Hence

$$A_{\mathrm{Theory}} = \eta_0^{\mathrm{CSV}} + \eta_A^p\tilde{G}_A^p + \eta_A^n\tilde{G}_A^n + \eta_E G_E^s + \eta_M G_M^s, \quad (22)$$
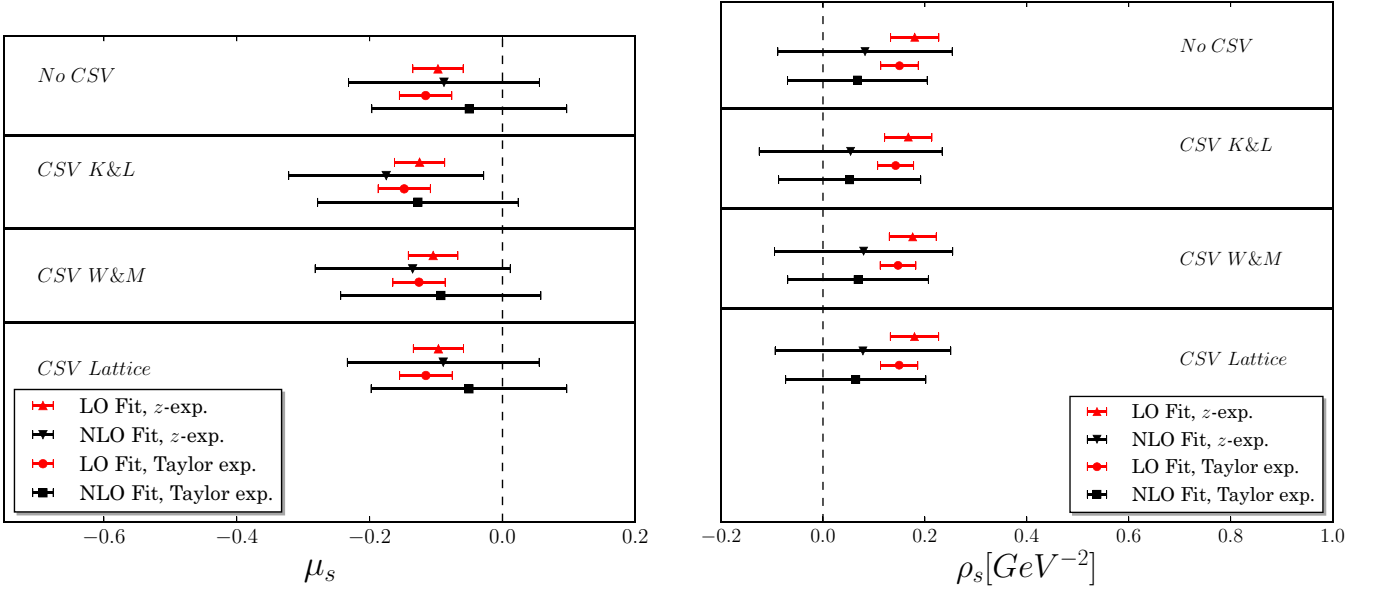
FIG. 5. Comparison of determinations obtained from the present work with and without CSV for the strange magnetic moment μ_s (left) and strange electric radius ρ_s (right). The leading-order fits are shown by the red (gray) points, and the next-to-leading-order fits by the black points.

where $\eta_0^{\text{CSV}} = \eta_0 + \eta_E^{\text{CSV}} G_E^{\text{CSV}} + \eta_M^{\text{CSV}} G_M^{\text{CSV}}$, with

$$\eta_{\text{CSV},E}^N = \left[\frac{G_F Q^2}{4\sqrt{2}\pi\alpha} \right] \cdot \left[\frac{\left(1 + R_V^n\right)\epsilon G_E^{\gamma,N}}{\epsilon \left(G_E^{\gamma,N}\right)^2 + \tau \left(G_M^{\gamma,N}\right)^2} \right], \qquad (23)$$

$$\eta_{\text{CSV},M}^N = \left[\frac{G_F Q^2}{4\sqrt{2}\pi\alpha} \right] \cdot \left[\frac{\left(1 + R_V^n\right)\tau G_M^{\gamma,N}}{\epsilon \left(G_E^{\gamma,N}\right)^2 + \tau \left(G_M^{\gamma,N}\right)^2} \right]. \qquad (24)$$

In the case of the PV asymmetry of ^{4}He, we should consider nuclear CSV, which we denote F^{CSV}, in addition to CSV at nucleon level, G_E^{CSV}. In this case, η_0^{CSV} can therefore be written as

$$\eta_0^{\text{CSV}} = \eta_0 + \left[\frac{G_F Q^2}{4\sqrt{2}\pi\alpha} \right] \cdot \left[-2F^{\text{CSV}} - 4 \frac{\left(1 + R_V^n\right)G_E^{\text{CSV}}}{G_E^p + G_E^n} \right], \qquad (25)$$

where in the notation of Ref. [28], $F^{\text{CSV}} \equiv F^{(1)}(q)/F^{(0)}(q) = -0.00157$ is used to calculate η_0^{CSV} for the theoretical PV asymmetry of ^{4}He at $Q^2 = 0.077$ and 0.091 GeV^2.

B. CSV theoretical works

To include effects of charge symmetry violation in our determination of the strangeness form factors, we consider three different calculations of the CSV form factors. The first work we consider is from Kubis and Lewis [16], denoted by "K&L CSV". They used effective field theory, supplemented with resonance saturation to estimate the relevant contact term, where the CSV is largely driven by ρ-ω mixing. To accomplish this, they employ a large ω-nucleon coupling constant $g_\omega \approx 42$ taken from dispersion analysis. Combining this estimate with calculations in HBχPT and infrared regularized baryon chiral perturbation theory, K&L predicted a CSV magnetic moment contribution $G_M^{\text{CSV}}(0) \equiv k^{u,d} = 0.025 \pm 0.020$, which includes an uncertainty arising from the resonance parameter. For the CSV slope parameters, K&L found

$\rho_M^{\text{CSV}} = -0.08 \pm 0.06$ GeV^{-2} and $\rho_E^{\text{CSV}} = -0.055 \pm 0.015$ GeV^{-2}. We take these values as our first estimate of the CSV form factors.

The second theoretical calculation of CSV we consider is from Wagman and Miller [17], denoted by "W&M CSV". In their work, they used relativistic chiral perturbation theory with a more realistic ω-nucleon coupling, i.e., $g_\omega \approx 10$. That study reported values of $G_M^{\text{CSV}}(0) = 0.012 \pm 0.003$, $\rho_M^{\text{CSV}} = 0.015 \pm 0.010$ GeV^{-2}, and $\rho_E^{\text{CSV}} = -0.018 \pm 0.003$ GeV^{-2}.

The third determination of the CSV form factor that we employ is based on an analysis of lattice QCD results [19], that we refer to as "Lattice CSV". The lattice study found significantly smaller values of the magnetic and electric CSV form factors compared to the previous two estimates. To study the effect of the CSV form factors obtained from lattice QCD, we summarize the results of Ref. [19] by $G_M^{\text{CSV}} = 0.000 \pm 0.001$ and $\rho_E^{\text{CSV}} = 0.000 \pm 0.001$ GeV^{-2}.

C. Strangeness with CSV

In order to propagate the uncertainties, we extend the covariance matrix above, Eq. (17), to include a correlated uncertainty associated with the theoretical estimates of CSV. For each theoretical description, we reanalyze the entire data set and present in Fig. 5 our determination of the strange magnetic moment μ_s (left) and strange electric radius ρ_s (right). Since the lattice CSV form factors are zero with a negligible uncertainty, they are consistent with the "No CSV" results. We also find no visible impact on μ_s and ρ_s from the inclusion of the W&M CSV form factors. Finally, when estimating the CSV form factors by the K&L parameters, we observe only small shifts in the central value of the strangeness magnetic moment. Nevertheless, even the worst case scenario of K&L does not appreciably affect the NLO fits.

V. CONCLUSION

We have presented a complete global analysis of all PVES asymmetry data for the proton, ^{4}He and deuterium. We have investigated the γZ exchange correction and the effect that CSV form factors have on the extraction of strange quark contribution. Including γZ box contribution in the analysis leads to small increases in the magnitude of the central values of μ_s and ρ_s when compared to results obtained without constraints from γZ exchange. CSV results considered in this work have tiny effects on the central values of the strangeness parameters, with the largest effect, while still small, coming from the inclusion of CSV form factors as provided by Kubis and Lewis [16]. Our results favor nonzero values for the strangeness magnetic moment and electric radius, with the most significant constraints coming from the LO fits using

a Taylor expansion for the strangeness form factors. Finally, in order to examine the model dependence of employing a Taylor expansion in our analysis, we also included fits using the z expansion, which were found to be in agreement.

The latest theory estimates on CSV are small, indeed small enough that they would not cloud the interpretation of future precision strangeness measurements. However, we note that the back-angle measurements do exhibit sensitivity to the effective axial form factor, presenting an opportunity for future investigation. The combined efforts to improve the resolution of strangeness, and reveal the structure of the anapole form factor offer the potential to establish a precision era of QCD and the nucleon. While further advancing the understanding of the mechanisms underlying nonperturbative QCD, such work will serve to gain further confidence in the use of lattice QCD for precision constraints in tests of the standard model.

TABLE IV. Values of η_i, appearing in Eq. (9), which describe the theoretical asymmetry for each experiment (in parts per 10^6). A^{phys} and δA are the measured asymmetry and the corresponding uncertainty, respectively, where the statistic and systematic error have been added in quadrature. While δA_{cor} is the correlated error in the G0 experiment [11,12], contributing to the second term in the covariance matrix, Eq. (17). Note that the back-angle G0 measurements (indicated by an *) are assumed to be uncorrelated with those at forward angle.

Experiment	Target	Q^2	θ	E	η_0	η_A^p	η_A^n	η_E	η_M	A^{phys}	δA	δA_{cor}	Ref.
SAMPLE	d	0.038	144	0.11	−2.13	0.46	−0.30	1.16	0.28	−3.51	0.81	0	[1]
SAMPLE	d	0.091	144	0.18	−7.02	1.04	−0.65	1.63	0.77	−7.8	1.0	0	[1]
SAMPLE	p	0.1	144	0.2	−5.50	1.57	0	2.11	3.45	−5.6	1.1	0	[2]
HAPPEX	p	0.477	12.3	3.35	−15.8	1.13	0	55.6	23	−15.1	1.1	0	[7]
PVA4	p	0.230	35.3	0.85	−5.78	0.88	0	22.4	5.08	−5.44	0.60	0	[3]
PVA4	p	0.108	35.4	0.57	−1.82	0.26	0	10.1	1.05	−1.36	0.32	0	[5]
G0	p	0.122	6.68	3.03	−1.93	0.06	0	11.9	1.17	−1.51	0.49	0.18	[11]
G0	p	0.128	6.84	3.03	−2.08	0.06	0	12.6	1.30	−0.97	0.46	0.17	[11]
G0	p	0.136	7.06	3.03	−2.28	0.07	0	13.4	1.47	−1.30	0.45	0.17	[11]
G0	p	0.144	7.27	3.03	−2.48	0.08	0	14.3	1.66	−2.71	0.47	0.18	[11]
G0	p	0.153	7.5	3.03	−2.73	0.09	0	15.3	1.89	−2.22	0.51	0.21	[11]
G0	p	0.164	7.77	3.03	−3.03	0.11	0	16.5	2.19	−2.88	0.54	0.23	[11]
G0	p	0.177	8.09	3.03	−3.41	0.13	0	17.9	2.58	−3.95	0.50	0.20	[11]
G0	p	0.192	8.43	3.03	−3.87	0.15	0	19.6	3.07	−3.85	0.53	0.19	[11]
G0	p	0.210	8.84	3.03	−4.45	0.19	0	21.7	3.72	−4.68	0.54	0.21	[11]
G0	p	0.232	9.31	3.03	−5.20	0.23	0	24.2	4.62	−5.27	0.59	0.23	[11]
G0	p	0.262	9.92	3.03	−6.29	0.31	0	27.8	6.03	−5.26	0.53	0.17	[11]
G0	p	0.299	10.6	3.03	−7.73	0.42	0	32.3	8.06	−7.72	0.80	0.35	[11]
G0	p	0.344	11.5	3.03	−9.61	0.58	0	38.0	11.0	−8.4	1.1	0.52	[11]
G0	p	0.410	12.6	3.03	−12.6	0.87	0	46.5	16.3	−10.3	1.1	0.6	[11]
G0	p	0.511	14.2	3.03	−17.6	1.49	0	60.1	27.0	−16.8	1.7	1.5	[11]
G0	p	0.631	16.0	3.03	−24.0	2.52	0	77.0	44.1	−29.0	1.7	1.3	[11]
G0	p	0.788	18.2	3.03	−33.1	4.45	0	100	74.6	−30.8	3.2	2.6	[11]
G0	p	0.997	20.9	3.03	−45.8	8.32	0	133	132	−38	12	0.52	[11]
HAPPEX	He^4	0.091	6.0	2.91	7.52	0	0	20.2	0	6.72	0.87	0	[6]
HAPPEX	p	0.099	6.0	3.03	−1.41	0.04	0	9.54	0.76	−1.14	0.25	0	[8]
HAPPEX	He^4	0.077	6.0	2.67	6.37	0	0	16.6	0	6.40	0.26	0	[9]
HAPPEX	p	0.109	6.0	3.18	−1.63	0.04	0	10.6	0.93	−1.58	0.13	0	[9]
PVA4	p	0.22	145	0.31	−13.3	3.47	0	2.88	11.1	−17.2	1.2	0	[4]
G0	p	0.221	110	0.35	−10.6	2.73	0	9.37	8.93	−11.3	0.9	0.43*	[12]
G0	d	0.221	110	0.35	−15.2	2.05	−1.38	7.63	2.21	−16.9	0.9	0.21*	[12]
G0	p	0.628	110	0.68	−36.9	11.9	0	19.7	62.2	−45.9	2.5	1.0*	[12]
G0	d	0.628	110	0.68	−50.7	8.46	−5.66	16.6	14.6	−55.5	3.9	0.7*	[12]
HAPPEX	p	0.624	13.7	3.48	−23.5	2.12	0	76.6	42.8	−23.8	0.9	0	[10]
PVA4	d	0.224	145	0.31	−18.6	2.50	−1.68	2.17	2.67	−20.1	1.4	0	[53]
Qweak	p	0.025	7.9	1.16	−0.22	0.01	0	2.27	0.05	−0.279	0.05	0	[20]

TABLE V. The $\Box_{\gamma Z}(E)$ ($\times 10^{-3}$) corrections evaluated for the measured proton PV asymmetry $A_{\rm PV}^p$ at forward angles.

Experiment	Q^2 (GeV^2)	E (GeV)	$\Box_{\gamma Z}(E)$ ($\times 10^{-3}$)
Qweak	0.025	1.165	5.120 ± 0.671
HAPPEx	0.099	3.030	7.205 ± 0.701
PVA4	0.108	0.570	2.843 ± 0.580
HAPPEx	0.109	3.180	7.250 ± 0.713
G0	0.122	3.030	6.969 ± 0.722
G0	0.128	3.030	6.907 ± 0.728
G0	0.136	3.030	6.825 ± 0.737
G0	0.144	3.030	6.742 ± 0.745
G0	0.153	3.030	6.648 ± 0.754
G0	0.164	3.030	6.534 ± 0.766
G0	0.177	3.030	6.398 ± 0.780
G0	0.192	3.030	6.243 ± 0.795
G0	0.210	3.030	6.056 ± 0.814
PVA4	0.230	0.850	3.257 ± 0.610
G0	0.232	3.030	5.831 ± 0.834
G0	0.262	3.030	5.527 ± 0.859
G0	0.299	3.030	5.161 ± 0.885
G0	0.344	3.030	4.733 ± 0.905
G0	0.410	3.030	4.143 ± 0.917
HAPPEx	0.477	3.350	3.749 ± 0.943
G0	0.511	3.030	3.340 ± 0.898
HAPPEx	0.624	3.480	2.740 ± 0.881
G0	0.631	3.030	2.547 ± 0.831
G0	0.788	3.030	1.753 ± 0.706
G0	0.997	3.030	1.038 ± 0.525

APPENDIX A: PARITY VIOLATING ASYMMETRIES

Table IV lists the asymmetries and their dependence on the leading unknown hadronic structure for all existing PVES experiments.

APPENDIX B: ENERGY DEPENDENCE OF THE γ-Z BOX

To incorporate the effect induced by the energy-dependent component of the γ-Z box radiative correction, the measured PV asymmetries given in Eq. (1) are modified by

$$A_{\rm PV\,corr}^p = A_{\rm PV}^p - \left[\frac{-G_F Q^2}{4\sqrt{2}\pi\alpha} \right] \Box_{\gamma Z}(E, Q^2) . \qquad (B1)$$

The forward (or vanishing momentum transfer) limit of this box are taken from Ref. [35], which extends Ref. [34] to also incorporate duality constraints. To estimate the momentum transfer dependence, we adopt the model suggested by Gorchtein *et al.* [36]:

$$\Box_{\gamma Z}(E, Q^2) = \Box_{\gamma Z}(E, 0) \frac{\exp(-BQ^2/2)}{F_1^p(Q^2)} , \qquad (B2)$$

with slope parameter estimated to be $B = 7 \pm 1$ GeV^2, and F_1^p the electromagnetic Dirac form factor of the proton. As adapted from the results presented in Ref. [54], the numerical values used in this work are summarized in Table V.

APPENDIX C: CORRELATION COEFFICIENTS

The fit parameters and correlations for the NLO z-expansion fit are shown in Table VI.

TABLE VI. Best-fit parameters for the NLO z-expansion fit (assuming charge symmetry) and corresponding correlation coefficients.

		$\tilde{g}_A^n$	μ_s	$\rho_{s,z}$	$\mu'_{s,z}$	$\rho'_{s,z}$
$\tilde{g}_A^p$	$-0.67(25)$	-0.43	-0.55	0.37	0.39	-0.24
$\tilde{g}_A^n$	$0.51(58)$		0.23	-0.16	-0.17	0.10
μ_s	$-0.09(14)$			-0.91	-0.98	0.85
$\rho_{s,z}$	$0.32(67)$				0.91	-0.96
$\mu'_{s,z}$	$-0.3(11)$					-0.93
$\rho'_{s,z}$	$3.6(55)$					

[1] E. J. Beise, M. L. Pitt, and D. T. Spayde, Prog. Part. Nucl. Phys. **54**, 289 (2005).

[2] D. T. Spayde *et al.* (SAMPLE Collaboration), Phys. Lett. **B583**, 79 (2004).

[3] F. E. Maas, P. Achenbach, K. Aulenbacher, S. Baunack, L. Capozza, J. Diefenbach, K. Grimm, Y. Imai, T. Hammel, D. vonHarrach, E. M. Kabuss, R. Kothe, J. H. Lee, A. Lorente, A. LopesGinja, L. Nungesser, E. Schilling, G. Stephan, C. Weinrich, I. Altarev, J. Arvieux, B. Collin, R. Frascaria, M. Guidal, R. Kunne, D. Marchand, M. Morlet, S. Ong, J. vandeWiele, S. Kowalski, B. Plaster, R. Suleiman, and S. Taylor (A4 collaboration), Phys. Rev. Lett. **93**, 022002 (2004).

[4] S. Baunack *et al.*, Phys. Rev. Lett. **102**, 151803 (2009).

[5] F. E. Maas *et al.*, Phys. Rev. Lett. **94**, 152001 (2005).

[6] K. A. Aniol *et al.* (HAPPEX collaboration), Phys. Rev. Lett. **96**, 022003 (2006).

[7] K. A. Aniol *et al.* (HAPPEX collaboration), Phys. Rev. C **69**, 065501 (2004).

[8] K. A. Aniol *et al.* (HAPPEX collaboration), Phys. Lett. **B635**, 275 (2006).

[9] A. Acha *et al.* (HAPPEX collaboration), Phys. Rev. Lett. **98**, 032301 (2007).

[10] Z. Ahmed *et al.* (HAPPEX collaboration), Phys. Rev. Lett. **108**, 102001 (2012).

[11] D. S. Armstrong *et al.* (G0 collaboration), Phys. Rev. Lett. **95**, 092001 (2005).

[12] D. Androic *et al.* (G0 collaboration), Phys. Rev. Lett. **104**, 012001 (2010).

[13] V. Dmitrašinović and S. J. Pollock, Phys. Rev. C **52**, 1061 (1995).

[14] G. A. Miller, Phys. Rev. C **57**, 1492 (1998).

[15] R. Lewis and N. Mobed, Phys. Rev. D **59**, 073002 (1999).

[16] B. Kubis and R. Lewis, Phys. Rev. C **74**, 015204 (2006).

[17] M. Wagman and G. A. Miller, Phys. Rev. C **89**, 065206 (2014); **91**, 019903(E) (2015).

[18] G. A. Miller, A. K. Opper, and E. J. Stephenson, Ann. Rev. Nucl. Part. Sci. **56**, 253 (2006).

[19] P. E. Shanahan, R. Horsley, Y. Nakamura, D. Pleiter, P. E. L. Rakow, G. Schierholz, H. Stüben, A. W. Thomas, R. D. Young, and J. M. Zanotti, Phys. Rev. D **91**, 113006 (2015).

[20] D. Androic *et al.* (Qweak collaboration), Phys. Rev. Lett. **111**, 141803 (2013).

[21] D. H. Beck, Phys. Rev. D **39**, 3248 (1989).

[22] R. D. Mckeown, Phys. Lett. **B219**, 140 (1989).

[23] M. J. Musolf, T. W. Donnelly, J. Dubach, S. J. Pollock, S. Kowalski, and E. J. Beise, Phys. Rep. **239**, 1 (1994).

[24] M. Tanabashi *et al.* (Particle Data Group collaboration), Phys. Rev. D **98**, 030001 (2018).

[25] J. Erler and S. Su, Prog. Part. Nucl. Phys. **71**, 119 (2013).

[26] T. W. Donnelly, J. Dubach, and I. Sick, Nucl. Phys. **A503**, 589 (1989).

[27] O. Moreno and T. W. Donnelly, Phys. Rev. C **89**, 015501 (2014).

[28] M. Viviani, R. Schiavilla, B. Kubis, R. Lewis, L. Girlanda, A. Kievsky, L. E. Marcucci, and S. Rosati, Phys. Rev. Lett. **99**, 112002 (2007).

[29] R. D. Young, J. Roche, R. D. Carlini, and A. W. Thomas, Phys. Rev. Lett. **97**, 102002 (2006).

[30] M. J. Musolf and B. R. Holstein, Phys. Lett. **B242**, 461 (1990).

[31] W. J. Marciano and A. Sirlin, Phys. Rev. D **27**, 552 (1983).

[32] M. Gorchtein and C. J. Horowitz, Phys. Rev. Lett. **102**, 091806 (2009).

[33] D. Androić *et al.* (Qweak collaboration), Nature (London) **557**, 207 (2018).

[34] N. L. Hall, P. G. Blunden, W. Melnitchouk, A. W. Thomas, and R. D. Young, Phys. Rev. D **88**, 013011 (2013).

[35] N. L. Hall, P. G. Blunden, W. Melnitchouk, A. W. Thomas, and R. D. Young, Phys. Lett. **B753**, 221 (2016).

[36] M. Gorchtein, C. J. Horowitz, and M. J. Ramsey-Musolf, Phys. Rev. C **84**, 015502 (2011).

[37] Z. Ye, J. Arrington, R. J. Hill, and G. Lee, Phys. Lett. **B777**, 8 (2018).

[38] V. Bernard, L. Elouadrhiri, and U.-G. Meissner, J. Phys. **G28**, R1 (2002).

[39] S.-L. Zhu, S. J. Puglia, B. R. Holstein, and M. J. Ramsey-Musolf, Phys. Rev. D **62**, 033008 (2000).

[40] R. E. Cutkosky and B. B. Deo, Phys. Rev. **174**, 1859 (1968).

[41] R. J. Hill and G. Paz, Phys. Rev. D **82**, 113005 (2010).

[42] Z. Epstein, G. Paz, and J. Roy, Phys. Rev. D **90**, 074027 (2014).

[43] R. González-Jiménez, J. A. Caballero, and T. W. Donnelly, Phys. Rev. D **90**, 033002 (2014).

[44] R. D. Young, R. D. Carlini, A. W. Thomas, and J. Roche, Phys. Rev. Lett. **99**, 122003 (2007).

[45] J. Liu, R. D. McKeown, and M. J. Ramsey-Musolf, Phys. Rev. C **76**, 025202 (2007).

[46] P. E. Shanahan, R. Horsley, Y. Nakamura, D. Pleiter, P. E. L. Rakow, G. Schierholz, H. Stüben, A. W. Thomas, R. D. Young, and J. M. Zanotti, Phys. Rev. Lett. **114**, 091802 (2015).

[47] R. S. Sufian, Y.-B. Yang, A. Alexandru, T. Draper, J. Liang, and K.-F. Liu (XQCD Collaboration), Phys. Rev. Lett. **118**, 042001 (2017).

[48] J. Green, S. Meinel, M. Engelhardt, S. Krieg, J. Laeuchli, J. Negele, K. Orginos, A. Pochinsky, and S. Syritsyn, Phys. Rev. D **92**, 031501(R) (2015).

[49] D. B. Leinweber, S. Boinepalli, I. C. Cloet, A. W. Thomas, A. G. Williams, R. D. Young, J. M. Zanotti, and J. B. Zhang, Phys. Rev. Lett. **94**, 212001 (2005).

[50] D. B. Leinweber, S. Boinepalli, A. W. Thomas, P. Wang, A. G. Williams, R. D. Young, J. M. Zanotti, and J. B. Zhang, Phys. Rev. Lett. **97**, 022001 (2006).

[51] P. Wang, D. B. Leinweber, A. W. Thomas, and R. D. Young, Phys. Rev. C **79**, 065202 (2009).

[52] O. Moreno, T. W. Donnelly, R. González-Jiménez, and J. A. Caballero, J. Phys. **G42**, 034006 (2015).

[53] D. Balaguer Ríos K. Aulenbacher, S. Baunack, J. Diefenbach, B. Glaser, D. vonHarrach, Y. Imai, E. M. Kabuss, R. Kothe, J. H. Lee, H. Merkel, M. C. MoraEspi, U. Muller, E. Schilling, C. Weinrich, L. Capozza, F. E. Maas, J. Arvieux, M. A. El-Yakoubi, R. Frascaria, R. A. Kunne, S. Ong, J. van de Wiele, S. Kowalski, and Y. Prok, Phys. Rev. D **94**, 051101(R) (2016).

[54] N. L. Hall, Hadron structure in electroweak precision measurements, Ph.D. thesis, University of Adelaide, School of Chemistry and Physics, 2014, https://librarysearch.adelaide.edu.au/permalink/61ADELAIDE_INST/18vpbuh/alma99276134069 01811.